Separation and Purification Technology 315 (2023) 123722

Contents lists available at ScienceDirect

Separation and Purification Technology

journal homepage: www.elsevier.com/locate/seppur

Dual-functionalized ionic liquid biphasic solvents with aqueous-lean for industrial carbon capture: Energy-saving and high efficiency

Jiaming Mao [a], Yanbin Yun [a,*], Meng Li [b], Wenli Liu [a], Chang Li [a], Liming Hu [a], Jia Liu [a], Lihua Wang [c,*], Chunli Li [d]

[a] College of Environmental Science and Engineering, Beijing Forestry University, Beijing 100083, PR China
[b] Beijing Synling Technology Co. Ltd, Beijing 100083, PR China
[c] Key Laboratory of Science and Technology on High-tech Polymer Materials, Institute of Chemistry, Chinese Academy of Sciences, Beijing 100190, PR China
[d] New Technique Centre, Institute of Microbiology, Chinese Academy of Sciences, Beijing 100101, PR China

ARTICLE INFO

Keywords:
Biphasic solvents
Ionic liquids
Poly (ethylene glycol) dimethyl ether
CO_2 capture
Energy efficiency

ABSTRACT

A novel, sustainable, dual-functionalized amino ionic liquid biphasic solvent of 3-(Dimethylamino)-1-propylamine-1,2,4-triazole/poly (ethylene glycol) dimethyl ether/water ([DMAPA][TZ]/NHD/water) was proposed for CO_2 capture to reduce the consumption of regeneration energy. Experimental results showed that the CO_2 absorption loading of the solvent was 1.95 mol $CO_2 \cdot L^{-1}$ solvent at a CO_2 partial pressure of 15 kPa. The volume of the CO_2-rich phase was 40 vol% of the total volume, with a loading of up to 4.65 mol $CO_2 \cdot L^{-1}$ solvent, accounting for approximately 95.4% of the blended CO_2 loading in the solvent. The CO_2-rich phase could be regenerated by 92.3% in 10 min at 373 K, without the presence of a lean phase. The regeneration efficiency of the solvent was maintained at 83% after 10 adsorption and desorption cycles. The reaction, regeneration, and phase-change mechanism were investigated using ^{13}C NMR and phase composition analysis. CO_2 reacted with [DMAPA][TZ] to form two kinds of carbamate during solubilization, and all carbamates could be further hydrolyzed to form HCO_3^- and CO_3^{2-}. The solvent effect, phase-change behavior, and CO_2 physical dissolution of NHD could promote the absorption and desorption rate and absorption capacity of CO_2. The energy consumption for CO_2 desorption could be reduced to 1.335 GJ·t^{-1} CO_2, which was 67% lower than that of 30 wt% ethanolamine (3.99 GJ·t^{-1} CO_2), given the lower heat of reaction, specific heat capacity, and solvent loss. Thus, this solvent presents a sustainable strategy for advancing carbon capture technologies.

1. Introduction

The combustion of fossil fuels in coal-fired power plants has resulted in the emission of large amounts of acidic gases, including CO_2, which has a high environmental impact and is the primary driver of the current climate change [1–3]. The post-combustion capture of CO_2, particularly through chemical absorption using aqueous solutions of alkanolamine, is considered to be the most effective and well-established method for CO_2 capture [4,5]. However, since such solutions are primarily composed of water, aqueous solutions of organic amines have a large specific heat capacity, and water evaporates during their heating and regeneration, resulting in high sensible heat of warming and latent heat of evaporation [6,7]. In terms of thermal power, the most commonly used 30 wt% ethanolamine (MEA) aqueous solution has a regeneration heat consumption of approximately 3.6~4.0 GJ·t^{-1} CO_2, and its capture cost is considerably higher than the target of $ 40·t^{-1} CO_2 [8,9]. Additionally, alkanolamine aqueous absorbents have problems such as high vapor pressure, high corrosion, easy scaling, and degradability [1,10]. To solve these problems, the design and development of absorption solvent systems with low vapor pressure, low energy consumption, low corrosiveness, and high absorption capacity are necessary [2,11–13].

Biphasic solvents for CO_2 trapping can be prepared by adjusting the solvent composition of alkanolamines [5,14,15]. This process had been extensively studied in CO_2 capture. Biphasic solvents are in a single phase before CO_2 absorption. However, once the absorption loading reaches a certain level, the solvents become liquid–liquid two-phase or liquid–solid two-phase due to the difference in solvent polarity and density [8,9]. In this state, only one phase is rich in CO_2, and the other

* Corresponding authors at: College of Environmental Science and Engineering, Beijing Forestry University, Beijing 100083, PR China (Y. Yun). Key Laboratory of Science and Technology on High-tech Polymer Materials, Institute of Chemistry, Chinese Academy of Sciences, Beijing 100190, PR China (L. Wang).
E-mail addresses: yunyanbin@bjfu.edu.cn (Y. Yun), wanglh@iccas.ac.cn (L. Wang).

https://doi.org/10.1016/j.seppur.2023.123722
Received 15 January 2023; Received in revised form 14 March 2023; Accepted 27 March 2023
Available online 31 March 2023

phase only has a small amount of dissolved CO_2. As a result, only the CO_2-rich phase needs to be regenerated, significantly reducing the energy required for regeneration [16]. Additionally, biphasic solvents can promote the CO_2 absorption reaction and improve the blend CO_2 loading due to the phase separation between the CO_2-rich phase and the unreacted solvent [1]. These split-phase solvents typically consist of a main solvent (primary or secondary amine) and solubilizing solvents (e.g., polyethylene glycol, ether, ethanol, sulfolane, and water) [14,15,17,18]. However, as the main absorbent is still an organic amine, the split-phase solvent has the same disadvantages as traditional absorbents, such as the volatilization of organic amines and organic solvents, high energy consumption for regeneration, and easy corrosion of metals. Therefore, the development of two-phase absorbents based on new solvents to overcome these problems has become a hot topic in carbon capture research [1].

Ionic liquids (ILs) can also be used to configure biphasic solvents due to their similar reaction mechanisms compared to alkanolamines [19]. However, ILs have more unique and better properties. As green solvents, ILs have an adjustable structure, very low vapor pressure, high thermal stability, low specific heat capacity, and moderate regeneration reaction heat [19–21]. Therefore, ILs are considered promising solvents for CO_2 capture and can be used instead of traditional alkanolamines to construct biphasic absorption solvents. In 2008, Camper et al. [22] demonstrated that homogeneous IL-MEA hybrid solutions formed insoluble carbamate precipitates after CO_2 absorption, and they separated the carbamate precipitates for regeneration. In 2020, Zhan et al. [8] synthesized a phase-change IL absorption system with [DETA][TZ] as the absorbent, and 1-propanol and water as cosolvents. In this system, the CO_2-rich phase accounted for 44 vol% of the total volume, and CO_2 loading reached up to 1.713 mol•mol^{-1}. Split-phase solvents are advantageous over aqueous organic amine solutions because they effectively reduce energy consumption and enhance absorption loading [1,23]. However, due to their low IL concentration (such as 0.5 mol·L^{-1}), the combined absorption load can still be increased [8]. IL biphasic solvents usually contain only a small amount of water or are completely anhydrous [24,25]. This characteristic avoids the use of organic amines and reduces the volatilization of amines and corrosion of equipment. However, the cosolvent is often ether, ethanol, n-propanol, and other organic solvents. The volatilization of organic solvents can make the absorbent susceptible to decomposition and the risk of combustion [1,17,25]. Also, the large amount of water in the flue gas can be enriched in the anhydrous absorbent, offsetting its advantages. Therefore, a water-lean solvent is a safer and more practical choice for CO_2 capture [1].

IL-based biphasic solvents have significant potential to save energy; however, they still have some limitations. For example, they often contain volatile and flammable organic cosolvents, have lower integrated absorption loading (unit in mol·L^{-1}), higher preparation costs, and require higher CO_2-rich phase volumes [8,12,26,27]. To achieve high regeneration efficiency, the IL-based biphasic solvents need the assistance of a CO_2-lean phase [16,17]. One promising solution is the use of dual-functionalized amino ILs (DFAILs) with aprotic heterocyclic anions (AHAs). DFAILs contain a large number of amino functional groups, which can chemically absorb large amounts of CO_2 to form carbamates. They can also be easily regenerated to release CO_2. AHAs can absorb CO_2 equimolarly without increasing the system viscosity [28,29]. Meanwhile, NHD exhibits very low vapor pressure (0.093 Pa, 298 K), viscosity ($5.8{\cdot}10^{-3}$ mPa·s, 298 K), and a specific heat capacity that is only half that of water (2050 J·kg^{-1}·K^{-1}) [30]. These characteristics have the potential to reduce solvent loss during regeneration, increase mass transfer efficiency, and reduce regeneration energy consumption. NHD also has a high solubility for acidic gases, such as CO_2, and is often used for industrial waste gas treatment. NHD is a primary constituent of Selexol®, a decarbonization and desulfurization solvent [31,32].

This study aimed to develop a novel dual-functionalized IL, namely, 3-(dimethylamine)-1-propylamine-1,2,4-triazole [DMAPA][TZ], and dissolve it in a mixed solution of NHD and water to prepare a new biphasic CO_2 capture solvent. The advantages of these solvents prompted the investigation of their potential. [DMAPA][TZ] possesses a large number of functional groups, and its absorption product, carbamate can be hydrolyzed to produce HCO_3^- and CO_3^{2-} further increasing the absorption load. NHD and a small amount of water (20 vol%) were used as cosolvents. NHD and water can be combined to promote reactions, regulate phase separation, reduce energy consumption for regeneration, and decrease solvent viscosity [9,24]. The experimental results, along with ^{13}C NMR analyzed to investigate the relationship between solvent properties, adsorption, desorption characteristics, mechanism, and regeneration energy consumption.

2. Materials and methods

2.1. Chemicals

3-(Dimethylamino)-1-propylamine (DMAPA), 1,2,4-triazole ([TZ]H), methanol-d_4 and DMSO-d_6 were supplied by Shanghai Macklin Biochemical Technology Co., Ltd. Poly (ethylene glycol) dimethyl ether (NHD, Mn = 250), ethanol, and ethanolamine (MEA) were provided by Shanghai Aladdin Biochemical Technology Co., Ltd. CO_2 (99.99%), and N_2 (99.99%) were purchased from Beijing Huanyu Jinghui Gas Technology Co., Ltd. All chemicals used were of analytical grade. Deionized water was used in all experiments, and all materials were used without further purification. Milli-Q system (Millipore Co., Ltd, USA) was used to produce deionized water (18.2 MΩ·cm^{-1}).

2.2. Synthesis of IL [DMAPA][TZ] and [DMAPA][TZ]/NHD/water

The dual-functionalized IL [DMAPA][TZ] was synthesized using a simple equimolar proton exchange method, as shown in Fig. S1. DMAPA and [TZ]H were prepared as concentrated solutions of 2 mol·L^{-1} each using water–ethanol (1:1 by volume) as the reaction solvent. The [TZ]H solution was added drop by drop to an equal mole amount of DMAPA solution under vigorous stirring. After the dropwise addition, stirring was continued overnight under 323 K to ensure sufficient semi-protonation of the organic amine. The mixture was heated to 343 K and evaporated under a vacuum in a rotary evaporator until no significant bubbles were produced. The product was collected and washed three times with ether to remove the unreacted amines or triazoles. The washed IL product was collected, placed in a vacuum drying oven, and dried overnight at 333 K. The final product was a viscous, colorless, and transparent liquid with a moisture content of less than 0.1% as determined by a Karl Fischer moisture tester. The ^{1}H NMR spectra of the [DMAPA][TZ] were recorded, and their structures are shown in Fig. S2. The spectra showed that the primary amine of DMAPA accepted the proton from [TZ]H, implying the successful synthesis of the IL [33,34]. To prepare the sample for testing, a certain amount of IL, NHD, and water were taken and stirred well as the sample to be tested.

2.3. CO_2 absorption and desorption

During the absorption process, the mixed gas (15% CO_2 + 85% N_2) was continuously provided to bubble into the solution and the flow velocity was set to 300 mL·min^{-1}. The absorption temperature was set at 303.15 K except when the effect of temperature on absorption was tested. 20 mL of solvent was taken for testing each time. A bubbling reactor with a capacity of 25 mL, a diameter of 2.2 cm, and a height of 16 cm was used for the absorption operation. The aeration tube was inserted into the reactor at a distance of 0.5 cm from the bottom of the reactor bottle, and the mouth of the tube had a glass sand core to optimize mass transfer efficiency. A photograph of the bubbling reactor is shown in Fig. S3b. Further details of the experimental and calculated procedures are provided in the Appendix-Supplementary information

between Figs. S3~S7 and Eqs. (S1)~(S9), named "Experimental and calculated procedures.".

2.4. Characterization

The viscosity-temperature curves of the solvents and IL were plotted using a rotary viscometer (Lichen NDJ-5S, China). The specific heat capacities of the IL [DMAPA][TZ] were determined using a differential scanning calorimeter (Netzsch DSC 200F3, Germany) by a standard sapphire method. The thermal stability of the IL was measured using a thermal gravimetric analyzer (Netzsch TG 209 F3, Germany). The carbon and hydrogen atom species of the solvents were evaluated using ^{13}C and ^{1}H NMR (AVIII 500 MHz, Bruker, Germany). Methanol-d_4 or DMSO-d_6 was used as a solvent for the deuterium lock, depending on the solubility of the solvent. The water contents of the ILs and [DMAPA][TZ]/NHD/water were determined using a Karl Fisher moisture meter (870 KF Titrino plus, Metrohm, Switzerland).

3. Results and discussion

3.1. Performance of CO_2 capture in the [DMAPA][TZ]/NHD/water

3.1.1. Screening of IL biphasic solvents

Based on the ^{1}H NMR spectra shown in Fig. S2, 1 mol of [DMAPA][TZ] has 1 mol of primary amines and 1 mol of a deprotonated secondary amine group from $[TZ]^-$, which can theoretically capture 1.5 mol of CO_2 per mole of IL [33,35]. The viscosity-temperature variation curves of [DMAPA][TZ] and their mixed solvents with NHD and water are shown in Fig. S8. As shown in Fig. S8, [DMAPA][TZ] had low viscosity, and the addition of water and NHD further reduced the viscosity of the solvents. These characteristics weakened the hydrogen bonding network between the IL and allowed for the accelerated mass transfer of CO_2 molecules [9]. However, the phase-change behavior of the solvents depended on the components of water and NHD. Therefore, in this section, the capacity and rate of CO_2 capture by mixed solvents were investigated at different volume ratios of water and NHD. To simulate the exhaust gas of thermal power, the composition of the feedstock gas was set to 15 vol% CO_2 + 85 vol% N_2, and the unit of absorption loading of the solvent was mol $CO_2 \cdot L^{-1}$ solvent. The results are shown in Fig. 1 and Table 1.

The CO_2 loading of the solvents increased with absorption time. During the experiments, the concentration of the IL was maintained at 30 vol% of the total solvent volume. The volumes of water and NHD were adjusted between 0 vol% and 70 vol% of the total volume, and the total solvent volume is 20 mL. Phase split occurred only when the ratio of V_{water}: V_{NHD} was between 1:6 and 3:4. The lower phase had a higher CO_2 loading. As the water content increased, the volume of the CO_2-rich phase gradually increased, and its loading gradually decreased. When the V_{water}: V_{NHD} ratio was 2:5, the overall solvent loading was 1.95 mol $CO_2 \cdot L^{-1}$ solvent, the loading of the lower phase was 4.65 mol $CO_2 \cdot L^{-1}$ solvent, accounting for 95.4% of the blend loading, and the CO_2-rich phase capacity was maximum. When the water content was 10 vol%, the CO_2-rich phase only accounted for 20 vol% of the total volume. Although the volume of the CO_2-rich phase was the smallest, the upper phase still had a certain capacity, indicating that some absorption products were dissolved in the upper phase and the phase separation was incomplete. After the water content was higher than 20 vol%, the proportion of the rich phase gradually increased until the absorption system did not undergo phase split after the water content reached 40 vol%. Therefore, the V_{water}: V_{NHD} ratio of 2:5 was the best ratio, and only the lower phase of the solution needed to be regenerated during the desorption process.

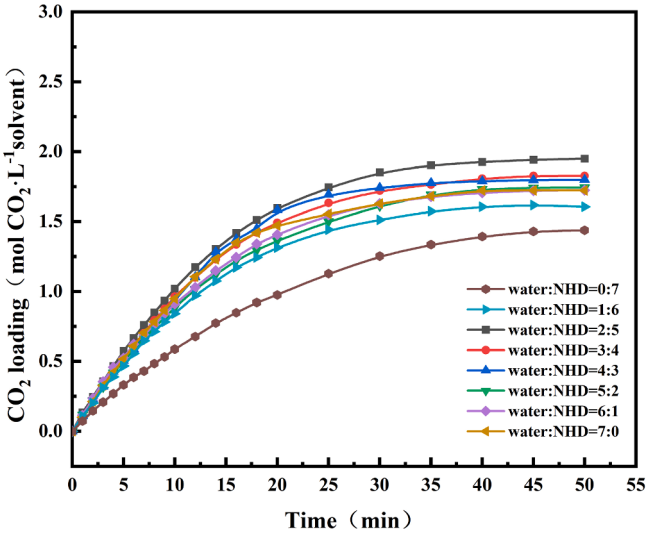

Fig. 1. CO_2 absorption in [DMAPA][TZ]/NHD/water at different volume ratios of water and NHD.

As shown in Table 1, the viscosity of the fresh solution decreased gradually with increasing water content, as the viscosity of water is lower than that of NHD. The viscosity of the solution after absorption was greater than before absorption, particularly for the rich-phase solution, which reached 70.7 mPa·s after absorption at V_{water}: V_{NHD} = 2:5. The absorption of CO_2 increased the viscosity of the amino IL due to hydrogen bonding [12,36].

The effect of different IL concentrations on the absorption loading at V_{water}: V_{NHD} = 2:5 is shown in Fig. 2. While increasing the total IL concentration from 30 vol% to 70 vol% raised the overall loading from 1.95 mol $CO_2 \cdot L^{-1}$ solvent to 2.65 mol $CO_2 \cdot L^{-1}$ solvent, the IL concentration increased by 2.3-fold, whereas the absorption loading increased only by 1.35-fold, which is not economically desirable. Therefore, we considered L30N50W20 solvent, consisting of 30 vol% IL: 50 vol% NHD: 20 vol% H_2O, as the optimal proportion of biphasic solvent, and used it in subsequent studies.

3.1.2. Effect of temperature on CO_2 capture in the [DMAPA][TZ]/NHD/water solvents

In CO_2 capture applications, CO_2 capture devices are typically installed after the flue gas desulfurization system, and the ambient temperature during capture is usually higher than at room temperature. Previous studies have shown that temperature has an important effect on the properties of phase-change solvents [12,25]. Therefore, the absorption performance of [DMAPA][TZ]/NHD/water was investigated in the temperature range between 303 K and 333 K. The results are shown in Fig. 3. As the temperature increased, the loading of CO_2 in the mixed solvent gradually decreased from 1.95 mol $CO_2 \cdot L^{-1}$ solvent to 1.43 mol $CO_2 \cdot L^{-1}$ solvent. This phenomenon was due to the exothermic nature of CO_2 absorption by ILs. An increase in temperature leads to the decomposition of the products of chemical absorption, resulting in a lower loading [27]. During the experiments, the [DMAPA][TZ]/NHD/water turned into a viscous gel-like object at 273 K, probably due to the low solubility of CO_2 absorption products at this temperature. This semisolid state hindered absorption. The results indicate that the absorption of [DMAPA][TZ]/NHD/water biphasic solvent is influenced by absorption temperature, and the optimal absorption temperature is 303 K.

3.1.3. Effect of CO_2 partial pressure on the CO_2 capture capacity of L30N50W20

The CO_2 loadings of L30N50W20 solvent at different CO_2 partial pressures (15~101 kPa) are shown in Fig. 4. The results indicate that increasing the CO_2 partial pressure could significantly enhance the CO_2 loading and absorption rate of the L30N50W20 solvent. As the CO_2 partial pressure increased from 15 kPa to 101 kPa, the CO_2 loading of the solvent increased from 1.95 mol $CO_2 \cdot L^{-1}$ solvent to 2.56 mol $CO_2 \cdot L^{-1}$ solvent. This increase in absorption could be attributed to the promotion

Table 1
Properties of [DMAPA][TZ]/NHD/water solvent with different volume ratios of water-NHD.

Volume ratio (water: NHD)	Phase separation	Lower volume (%)	Fresh viscosity (mPa·s)	Saturated Viscosity (mPa·s)			CO_2 loading (mol CO_2·L^{-1} solvent)		
				Blend	Upper	Lower	Blend	Upper	Lower
0:7	N	/	8.1	23.2	/	/	1.44	/	/
1:6	Y	20	8.0	/	7.5	73.7	/	0.86	4.56
2:5	Y	40	7.9	/	5.2	70.7	/	0.15	4.65
3:4	Y	50	7.4	/	4.9	28.2	/	0.09	3.55
4:3	N	/	6.8	20.3	/	/	1.80	/	/
5:2	N	/	6.2	18.7	/	/	1.75	/	/
6:1	N	/	5.6	15.9	/	/	1.72	/	/
7:0	N	/	5.1	15.4	/	/	1.72	/	/

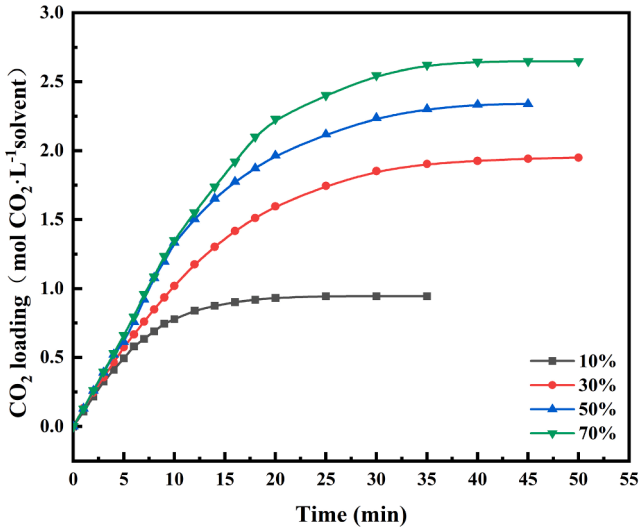

Fig. 2. CO_2 absorption into [DMAPA][TZ] at different IL volume ratios.

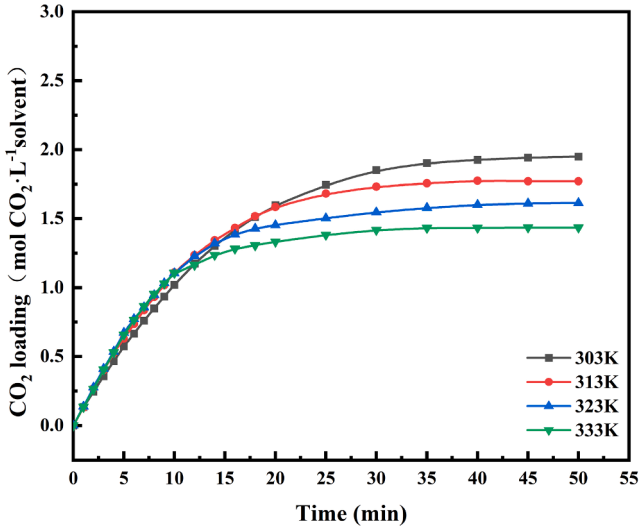

Fig. 3. CO_2 absorption in L30N50W20 at different temperatures.

of the shift of the absorption chemical equilibrium to the right by an increase in CO_2 partial pressure.

3.1.4. Phase split behavior of [DMAPA][TZ]/NHD/water

Understanding the relationship between phase split behavior and absorption performance is critical for developing efficient absorbents. The phase split behavior of [DMAPA][TZ]/NHD/water during CO_2 absorption is illustrated in Fig. S9, while a photograph of the solvent is shown in Fig. 5. At the beginning of absorption (<10 min), the solution remained homogeneous. However, as the absorption loading reached 1.02 mol CO_2·L^{-1} solvent, the solution became turbid and separated into two liquid–liquid phases upon standing. The viscosities of the upper and lower phases were different, and the volume of the CO_2-rich phase remained constant after the phase separation occurred. However, the CO_2-rich phase accounted for only 40% of the total volume, indicating that CO_2 was mainly enriched in the lower phase. Consequently, only the lower phase required regeneration after reaching saturation, leading to lower regeneration costs. This result suggests that biphasic solvents have great potential for energy saving in industrial carbon capture processes [7,18].

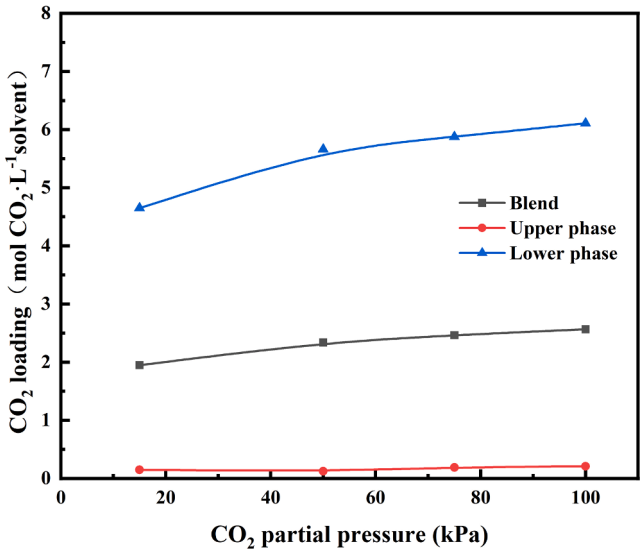

Fig. 4. CO_2 absorption into L30N50W20 at different CO_2 partial pressures.

Changes in the conductivity of the upper/lower phases during absorption were measured separately using a conductivity meter with a 10-times diluted aqueous solution. The changes in the absorption load and conductivity of the upper/lower phases with time are shown in Fig. 6. The test process revealed that both phases were soluble in larger amounts of water, which may be due to water solvation. When the absorption reached saturation, the conductivity of the lower phase aqueous solution reached 7420 μs·cm^{-1}, while the conductivity of the upper phase aqueous solution was only 378 μs·cm^{-1} (after diluting 10 times). This phenomenon indicated that a large amount of IL was located in the lower phase, while the IL concentration in the upper phase was lower. During the absorption after the phase change, the ion concentration in the upper and lower phases showed fewer changes, indicating that the phase migration of ions was smaller after the phase change occurred. This phenomenon may be due to the principle of similar phase solubility, in which the unreacted IL also tended to migrate to the rich

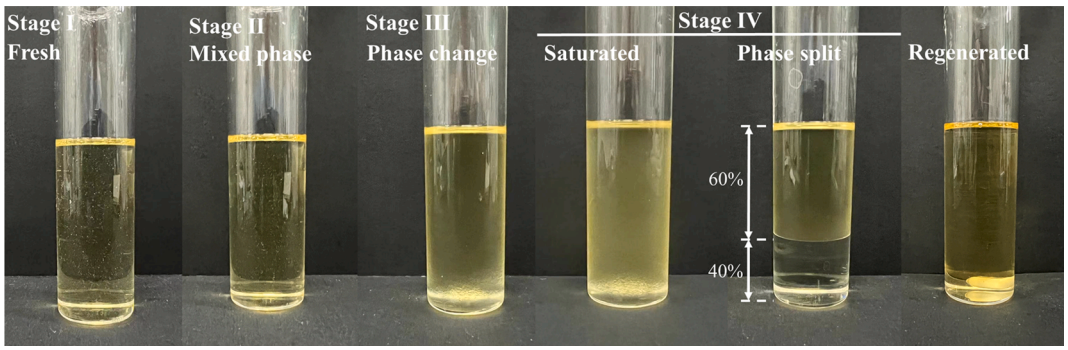

Fig. 5. Optical photograph of the L30N50W20 solvent during the absorption process.

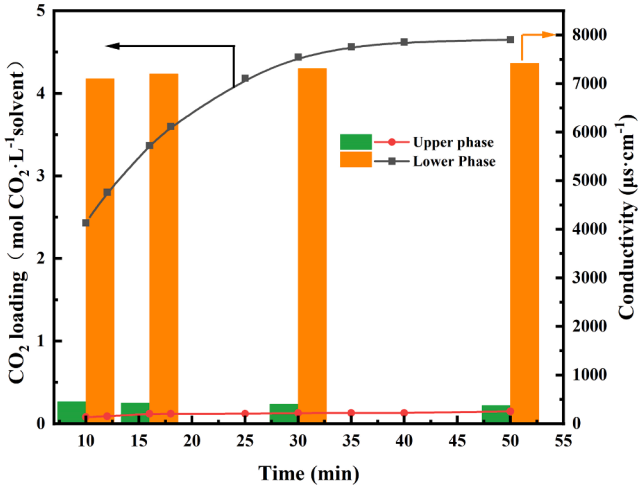

Fig. 6. The relationship between conductivity, loading, and absorption time of the upper and lower phases.

phase and reach dissolution equilibrium with the CO_2-lean phase after the phase change occurred. The water contents of the upper and lower phases after the phase change were subsequently measured using a Karl Fischer moisture tester. The results are shown in Fig. 7. During the absorption after the phase change, the water content of the upper phase decreased from 10.53% to 9.6%, while that of the lower phase increased from 29.61% to 30.55%. Wang et al. [20] showed that CO_2 could be used as a switch to modulate the polarity of ILs. In this study, the polarity of [DMAPA][TZ] changed after interaction with CO_2. The interactions between the absorption products and the solvent were mainly hydrogen bonds and van der Waals forces [9]. The phase split indicated that the dipole moment between the absorption products and water was higher than that between absorption products and NHD [37]. This result was primarily due to an increase in dipole moment with the polarity of the solvent and the interaction between the solvent molecules and the compound, which is the main reason for the phase transition. Therefore, the upper phase contained a small amount of IL and a small amount of water, while the lower phase contained absorption products of IL and a large amount of water when it reached saturation. The upper and lower phase compositions and absorption products will be further analyzed later using ^{13}C NMR spectroscopy in section 3.2.3.

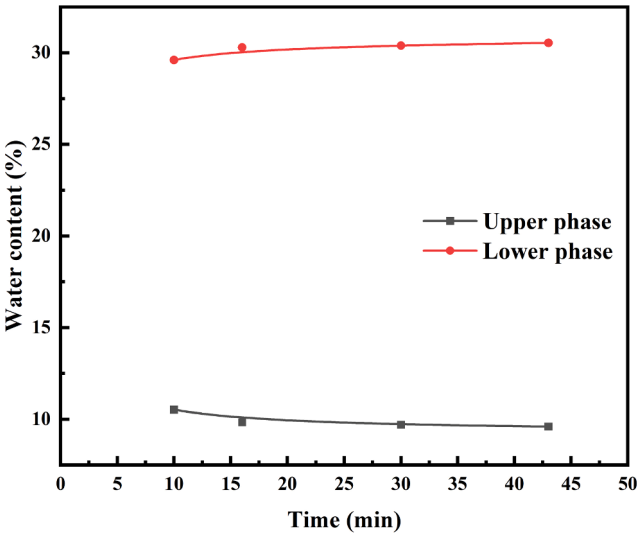

Fig. 7. Water content versus adsorption time.

3.1.5. *Desorption performance of the saturated CO_2-rich phase*

Studying the desorption performance of saturated solvents is a crucial criterion for absorbents. When the solvent reaches saturation, it splits into two liquid–liquid phases, and only the lower phase of the solution needs to be regenerated. To prevent the decomposition of IL during thermal desorption, thermogravimetric analysis of the IL was performed, and the results are shown in Fig. S10. The decomposition onset temperature was 433 K, which was considerably higher than the desorption operation temperature of the solution. The CO_2-rich phase was separated using a partition funnel and desorbed in an oil bath at 343~373 K, and the results are shown in Fig. 8. The regeneration efficiency of the solvent increased with the desorption temperature and

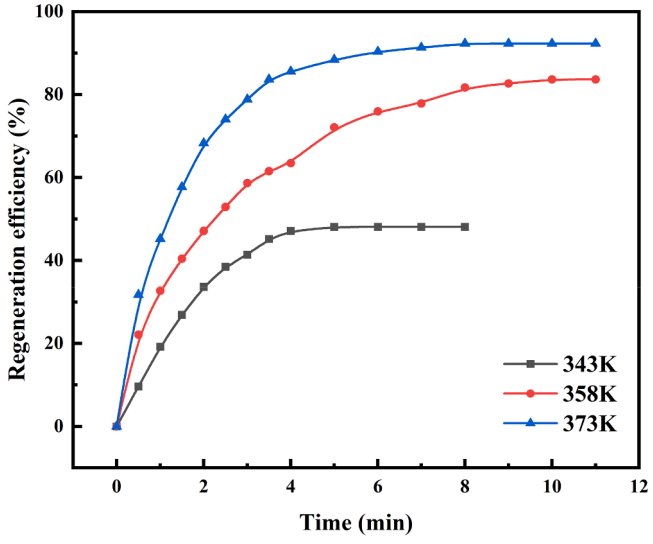

Fig. 8. Regeneration efficiency of the CO_2-rich phase from L30N50W20 at different temperatures.

desorption time. At 343 K, the regeneration efficiency of the lower phase solution was lower than 50% when the desorption reached equilibrium, although the time to reach desorption equilibrium was shorter (within 5 min). With the increase in desorption temperature, the desorption time to reach the desorption equilibrium was 10 min at 373 K, and the highest desorption efficiency could reach 92.3%. The desorption temperature and desorption time were significantly lower than those of the saturated MEA aqueous solution, and the system had a very high desorption rate. The high desorption rate may be due to the low stability of the absorption products and their easy decomposition. Moreover, the CO_2-rich phase used in this experiment was less, and the device heats up faster. Therefore, considering the energy saving and high efficiency of the system, the optimal regeneration conditions for the CO_2-rich phase were 373 K and 10 min.

To evaluate the long-term cycling stability of the solution, repeated absorption–desorption at a regeneration temperature of 373 K was performed. As shown in Fig. 9, the regeneration efficiency of the solvent slightly decreased as the number of regeneration cycles increased. However, even after the 10th regeneration, the solvent was still able to maintain 83% of the initial absorption efficiency. The initial regeneration efficiency decreased to 92.3% after the first absorption, which was due to the presence of some absorption products in the solvent that was more difficult to regenerate at that regeneration temperature. The results indicate that the absorbent could still be reused after several thermal desorptions.

As mentioned above, biphasic solvents based on ILs have lower viscosity, higher capacity, lower regeneration temperature and energy consumption, and less solvent loss compared to traditional phase change solvents. These advantages can significantly reduce energy loss.

3.2. Mechanism of CO_2 capture in [DMAPA][TZ]/NHD/water solvents

3.2.1. ^{13}C NMR analysis of the absorption process

Fig. 10 shows the ^{13}C NMR signals of various carbon-containing substances, such as hydrocarbon groups, two kinds of carbamate (–NHCOO$^-$ and [TZ]COO$^-$), and carbonate/bicarbonate (CO_3^{2-}, HCO_3^-). The absorption process was divided into four stages based on the phase change behavior of the solvent and the absorption loading, as shown in Fig. 5. For the fresh solvent (Stage I), the signals at 40.28 ppm (C1), 28.88 ppm (C2), 58.07 ppm (C3), 45.44 ppm (C4), and 148.54 ppm (C5) in Fig. 10a were designated as IL [DMAPA][TZ], while the characteristic peaks of NHD appeared at 59.08 ppm (C6), 71.47 ppm (C7), and 72.90 ppm (C8) [9,38]. As shown in Fig. 10b, in stage II of CO_2 absorption, the solvent remained in a clear and transparent state and did not exhibit phase separation. At this stage, two faint new peaks could be observed at 165.65 ppm (Ca') and 161.20 ppm (Cb'), indicating carbamate from DMAPA (–NHCOO$^-$) and carbamate from [TZ]$^-$ ([TZ]COO$^-$), respectively [12,24]. The ^{13}C NMR peaks of some hydrocarbon groups were slightly split and shifted, possibly due to changes in the molecular charge caused by carbamate and protonated amine formation [24].

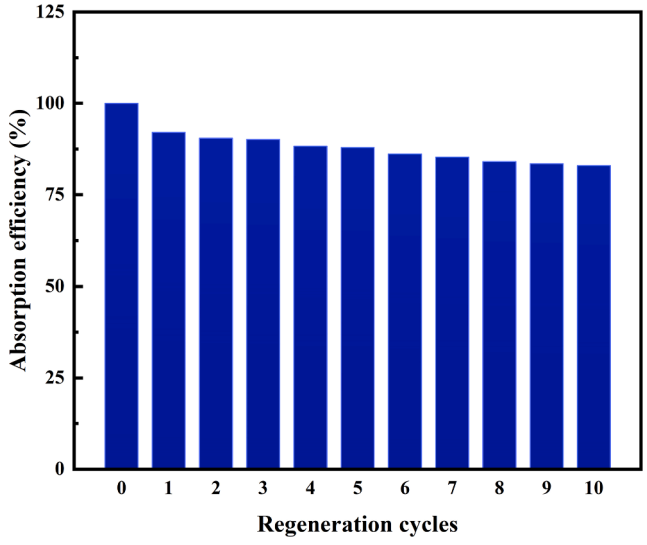

Fig. 9. Recycling of biphasic solvent for CO_2 absorption.

As the CO_2 absorption loading increased, the solvent gradually became turbid, and the absorption entered stage III, where the solvent underwent phase separation, but the absorption did not reach saturation, as shown in Fig. 10c. The intensity of the characteristic peaks of [DMAPA][TZ] in the upper phase and NHD in the lower phase showed a relative decreasing trend. A new peak formed at 162.06 ppm (Cc') at this stage, which could be attributed to the formation of CO_3^{2-}/HCO_3^-, which may be due to the hydrolysis of carbamate or the direct reaction of CO_2 with water [8]. When the CO_2 absorption reached saturation (Fig. 10d), the carbamate and bicarbonate signals in the lower phase were further enhanced, and no peaks associated with carbamate or bicarbonate in the upper phase were found. This result proved that the products of CO_2 absorption were mainly concentrated in the lower phase. Compared to a previous study, the upper phase mainly consisted of a small amount of water, a large amount of NHD, and a small amount of unreacted IL. In contrast, the lower phase mainly consisted of water, products of the reaction between CO_2 and [DMAPA][TZ], and a small amount of NHD. The ^{13}C NMR spectrum did not show any evidence of NHD involvement in the chemical reaction, and NHD was mainly used as a solvent for phase separation and to assist in the enrichment of CO_2.

3.2.2. ^{13}C NMR of the desorption process

The ^{13}C NMR spectra of the CO_2-rich phase at 3 and 10 min of regeneration are shown in Fig. 11. The decomposition of carbamate, carbonate, and bicarbonate was represented by the chemical shifts from 160 ppm to 168 ppm, where the alterations were mostly concentrated. The signal of the CO_2 absorption product only survived from carbamate on the cation (–NHCOO$^-$) and very faintly from carbamate on [TZ]$^-$ ([TZ]COO$^-$) during the desorption time of 3 min, and the signal of CO_3^{2-}/HCO_3^- vanished. This result proved the ease of decomposition of the absorption product as HCO_3^-/CO_3^{2-} > [TZ]COO$^-$ > –NHCOO$^-$. Similar to the results by Zhan et al. [8], the ΔH_{abs} of [TZ]COO$^-$ decomposition reaction was smaller and easier to decompose than –NHCOO$^-$. The peak representing –NHCOO$^-$ increased slightly during the desorption process, indicating that some of the released CO_2 were trapped by the cation of IL. As the desorption time was extended to 10 min, only a small amount of Cc' (–NHCOO$^-$) was present, which was in agreement with the results of the desorption experiment. Therefore, this demonstrated that the present solvent could achieve high regeneration efficiency quickly in the presence of only the rich phase. Contradictory results were obtained from the studies of Zhan et al. [8], Kong et al. [17], and Huang et al. [16], where the regeneration of the CO_2-rich phase required the participation of a certain amount of the CO_2-lean phase. The discrepancy may be related to the small amount of NHD in the CO_2-rich phase, which can be found in the ^{13}C NMR pattern of stage IV; the absorption products were easily decomposed. Moreover, the CO_2 product signal positions in the ^{13}C NMR spectra during absorption and desorption were the same as during absorption, but the signal intensity changed in the opposite direction. This phenomenon was due to thermal desorption being the reverse process of absorption. The slight variation at 148.45 ppm (C5) may be due to following reasons: [TZ]$^-$ may have two types of tautomers. In the CO_2 absorption process, two types of tautomers were gradually converted to the same type. However, with the desorption of CO_2, the tautomer of [TZ]$^-$ was again converted from one type to two. Due to the superposition of the signals from two tautomers, the chemical shift at 148.45 ppm broadens and the peak decreases as the desorption process proceeds.[12,25].

Chen et al. [9] showed that NHD could significantly reduce the energy barrier for CO_2 uptake and regeneration due to the solvent effect of

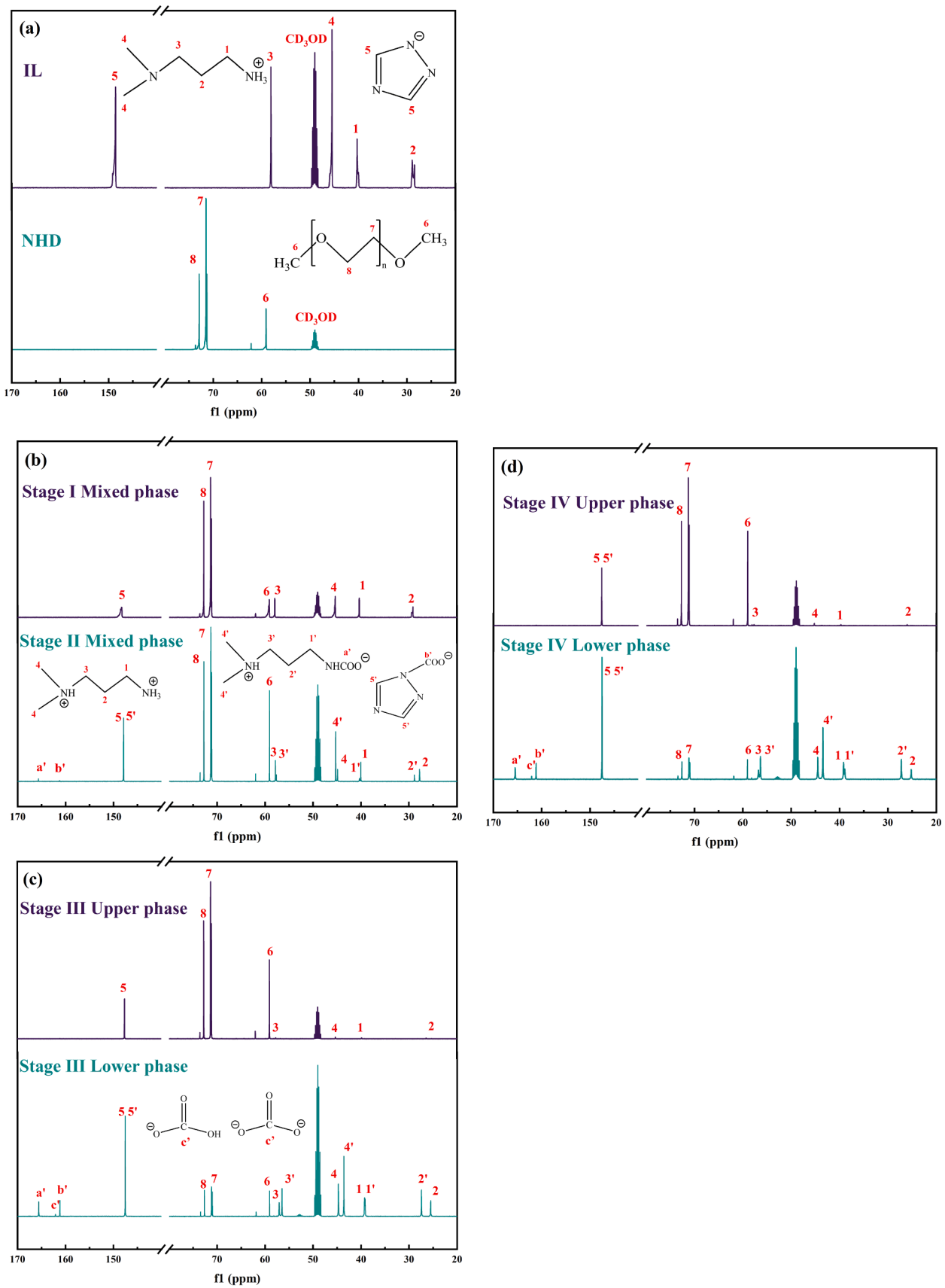

Fig. 10. ^{13}C NMR spectra of [DMAPA][TZ]/NHD/water during the absorption process: (a) IL and NHD; (b) fresh solvent (Stage I) and absorbent without phase separation (stage II); (c) after phase change but not saturated (stage III); and (d) saturated solvent (stage IV).

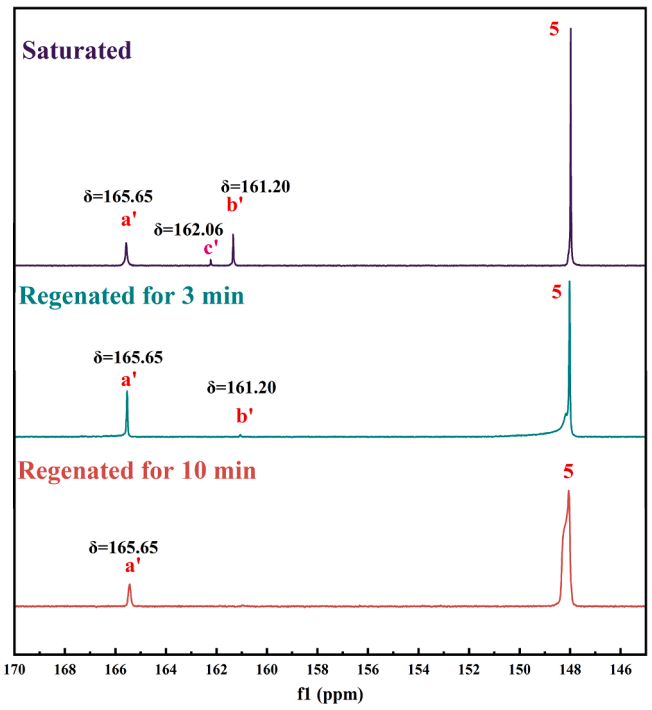

Fig. 11. ^{13}C NMR spectra of the desorption process.

NHD. The H_2O molecules had a higher polarity than NHD molecules, leading to more stable hydrogen bonds between H_2O and IL molecules. These hydrogen bonds reduce the charge density around the N atom, decreasing the nucleophilicity or alkalinity of $[TZ]^-$ or $[DMAPA]^+$. After the induction of NHD, these hydrogen bonds can be weakened, favoring the decomposition reaction of the carbamate [9]. In addition, the energy barrier of the decomposition reaction of $[TZ]COO^-$ was lower than that of the $–NHCOO^-$ due to the aromatic nature of the triazole. In the [TZ]H molecule, 1-N is sp^2 hybridization, and the [TZ]H had aromaticity. Strong electronegativity between 2-N and 4-N enabled the unpaired electrons on 1-N to participate in ring conjugation, which decreased the electron cloud density at 1-N, increased the eletronegativity, reduced the energy of the N–H bond, and made 1-H readily depart as a proton. The carbamate produced at 1-N (N–C bond), based on the same theory and with the same high electronegativity carbamate group, was unstable and readily decomposed. The alkyl group had strong electropositivity, whereas the cation produced carbamate, which increased the electronegativity on N. The difference between carbamate and alkyl group's electron-giving properties were significant, thus, not easily decomposed [20,28]. In addition, the reaction of the anion with CO_2 does not need to go through proton transfer, and its reaction and decomposition rate is much faster. This phenomenon explains why the solvent described in this study was easily regenerated.

3.2.3. CO_2 absorption, desorption, and split phase mechanism of L30N50W20

Based on the above experiments and the results of ^{13}C NMR analysis of the CO_2-rich phases, the mechanism of CO_2 trapping and phase separation of the solution could be summarized as follows. Each mole of [DMAPA][TZ] contained 1 mol of the primary amine group and 1 mol of secondary amine anion form $[TZ]^-$ capable of absorbing CO_2 in equal amounts. Thus, 1 mol of [DMAPA][TZ] absorbed 1.5 mol of CO_2 and ensured the loading of CO_2. In the absorption system, the high solubility of CO_2 in the NHD increased the partial pressure of CO_2 in the system, which promoted the shift of absorption equilibrium to the right. The carbamate could be hydrolyzed to produce HCO_3^-/CO_3^{2-}, further enhancing the blend absorption load. In addition, the split-phase behavior of the solvent could separate the absorption products from the unreacted IL and promote the absorption reaction. The system's $[DMAPA]^+$ and $[TZ]^-$ reacted with CO_2 first. During the reaction, the protonated primary amine on the IL cation transferred the proton to the tertiary amine for the primary amine to participate in the reaction [33]. Then, the primary amine reacted with CO_2 to form the amphoteric ion and produced the carbamate through the amphoteric ion reaction mechanism. Moreover, a significant number of protons were moved during the synthesis of carbamate on cations. Nevertheless, the proton transfer process is the reaction's rate-limiting phase. The water in the system was amphoteric and effectively assisted the proton transfer as an excellent proton acceptor and donor, which was one of the reasons for the solvent's high absorption rate and absorption capacity [39,40]. In contrast, the reaction of anions with CO_2 did not need to undergo proton transfer, facilitating the reaction rate. The solventization of NHD also helped reduce the free energy of activation of carbamate formation and improve the solvent absorption capacity.

Reaction of IL cations with CO_2 (R1: $-CH_3$, R2: $-CH_2-CH_2-CH_2-$):

$$R1_2N\text{-}R2NH_3^+ + CO_2 \rightarrow R1_2HN^+\text{-}R2NH_2^+COO^-(1)$$

$$R1_2HN^+\text{-}R2NH_2^+COO^- + R1_2N\text{-}R2NH_3^+ \rightarrow R1_2HN^+\text{-}R2NHCOO^- + R1_2HN^+\text{-}R2NH_3^+(2)$$

One zwitterion could hydrolyze with two H_2O molecules [41]:

$$R1_2HN^+\text{-}R2NH_2^+COO^- + H_2O \rightarrow R1_2HN^+\text{-}R2NHCOO^- + H_3O^+(3)$$

$$R1_2HN^+\text{-}R2NHCOO^- + H_2O \rightarrow R1_2N\text{-}R2NH_3^+ + HCO_3^-(4)$$

AHAs could react with CO_2 to form carbamates equimolarly, giving them a higher CO_2 loading capacity than alkanolamine. The reaction equation of the IL anion with CO_2 was as follows.

$$[TZ]^- + CO_2 \rightarrow [TZ]COO^-(5)$$

$[TZ]COO^-$ and $-R2NHCOO^-$ could be hydrolyzed with water to form CO_3^{2-} and HCO_3^-. The reactions are as follows[24]:

$$[TZ]COO^- + H_2O \rightarrow [TZ]H + HCO_3^-(6)$$

$$R1_2HN^+\text{-}R2NHCOO^- + H_2O \rightarrow R1_2N\text{-}R2NH_3^+ + HCO_3^-(7)$$

$$R1_2HN^+\text{-}R2NHCOO^- + [TZ]H + H_2O \rightarrow R1_2N\text{-}R2NH_3^+ + [TZ]^- + HCO_3^- + H^+(8)$$

The change in solution pH during the absorption process is shown in Fig. S11. Since the system was alkaline in the absorption process, OH^- could also react directly with CO_2 to form HCO_3^-:

$$OH^- + CO_2 \rightarrow HCO_3^-(9)$$

The $R1_2N\text{-}R2NH_3^+$ and [TZ]H molecules generated after hydrolysis underwent proton transfer to generate $[TZ]^-$, which participated in the subsequent reactions. Thus, the added water acted as an excellent proton transfer medium to promote the reaction. On the other hand, such a step promoted carbamate hydrolysis to generate CO_3^{2-}/HCO_3^- to improve the solvent's absorption load. Finally, water and NHD acted as phase separation promoters to ensure the phase change of the whole system, which was the reason for the absorption system's high absorption load and absorption/desorption rate. Contrary to Zhan et al. results, carbamates formed from non-protonic heterocyclic anions could be detected in this study ^{13}C NMR of the rich phase after absorption. Zhan et al. [8] pointed out that such carbamates were easily hydrolyzed, and only [TZ]H was present in the CO_2-rich phase of the product. This phenomenon may be due to the enrichment of CO_2 by NHD, which corresponded to an increase in the partial pressure of CO_2, facilitating the reaction and making the product. Oncsik et al. [35] suggested that the cations of [DMAPA][TZ] ILs did not react with CO_2. However, in the current investigation, the cations could also produce amine carbamate, contributing to the solvent's high absorption load. This result may be explained by the enrichment of CO_2, the lowering of the energy barrier

caused by NHD, and the protons being transferred by water.

After absorption, the products enriched in the lower phase were –NHCOO$^-$ (from [DMAPA]$^+$), [TZ]COO$^-$, and HCO_3^-/CO_3^{2-}. The absorption products were mainly bound to water and concentrated in the lower phase because carbamates were more polar and aggregated in the aqueous phase than in the NHD. Also, the enhancement of hydrogen bonding between solute and water led to a decrease in the solubility of the carbamate in NHD [2]. A small fraction of the unreacted IL remained in the upper phase because of the similar polarities of water and NHD. A small amount of NHD was present in the lower phase, probably due to its role as a phase splitter during absorption.

Thermal desorption can be considered as the inverse of absorption, and the reaction is as follows:

$$CO_3^{2-} + 2H^+ \rightarrow H_2O + CO_2 (10)$$

$$HCO_3^- + H^+ \rightarrow H_2O + CO_2 (11)$$

$$[TZ]COO^- \rightarrow [TZ]^- + CO_2 (12)$$

$$R1_2HN^+\text{-}R_2NH_3^+ + R1_2N^+\text{-}R2NHCOO^- \rightarrow 2\ R1_2N\text{-}R2NH_3^+ + CO_2 (13)$$

Reaction (13) can be divided into cation deprotonation and carbamate reception proton decomposition. Proton transfer is the rate-limiting step in CO_2 desorption and requires a lot of energy [42,43].

$$R1_2HN^+\text{-}R_2NH_3^+ + HCO_3^- \rightarrow R1_2N\text{-}R2NH_3^+ + H_2CO_3 (14)$$

$$R1_2HN^+\text{-}R_2NH_3^+ + H_2O \rightarrow R1_2N\text{-}R_2NH_3^+ + H_3O^+ (15)$$

$$R1_2HN^+\text{-}R2NHCOO^- + H_3O^+ \rightarrow R1_2HN^+\text{-}R2NH_2^+COO^- \rightarrow R1_2N\text{-}R2NH_3^+ + CO_2 (16)$$

Therefore, the CO_2 capture and separation mechanism is shown in Fig. S12. CO_2 was mainly absorbed by [DMAPA][TZ] to form carbamate, HCO_3^- and CO_3^{2-}. The CO_2 product was enriched in the lower phase due to the different polarity and densities of the product and solvent, whereas the NHD was in the upper phase due to its lower density. Therefore, NHD and water were present as phase separators promoting phase separation. During absorption and desorption, NHD acted as an activator to lower the reaction energy barrier and enhance absorption and regeneration performances.

3.3. Heat duty of CO_2 capture into [DMAPA][TZ]/NHD/water

3.3.1. Specific solvent loss (SSL)

The SSL is an important index to evaluate the desorption performance of the absorbent. This index is defined as the molarity loss of solvent per unit mole of CO_2 vapor extracted. Fig. S13 displays the SSLs of different absorbent solvents. The SSL value of the rich liquid was 0.41 mol solvent·mol^{-1} CO_2, which was lower than that of 30 wt% MEA aqueous solution. This result was caused by the vapor pressure of ILs and NHD, which was very low and almost negligible. The water content of the rich phase was 30%, which was half that of the aqueous MEA solution.

Meanwhile, the rich phase only needed to be desorbed at 373 K, and the low desorption temperature was also beneficial in reducing solvent loss. Finally, the CO_2-rich phase only constituted 40% of the entire volume, and the phase change solvent was only needed to desorb the rich phase. The loading of the CO_2-rich phase was higher than that of the MEA aqueous solution. These results further illustrated the system's higher desorption efficiency.

3.3.2. Evaluation of the heat duty

Based on Equations (S5)~(S7), the reaction enthalpies (ΔH_{abs}) of CO_2 absorption in the biphasic solvents could be calculated using vapor–liquid equilibrium (VLE) curves shown in Fig. S14. The measured temperatures were 303.15 K and 313.15 K. For comparison; the 30 wt% MEA was performed as a control test. The VLE values demonstrated the reliability of the experimental results for MEA being comparable to those published in the literature. The partial pressure of CO_2 rose with increasing CO_2 loading and temperature, and the VLE curve showed an inverted S-shape. The regeneration heat duty of 30 wt% MEA and L30N50W20 are demonstrated in Fig. 12. According to Wang et al. [14], the regeneration heat duty of 30 wt% MEA was 3.99 GJ·t^{-1} CO_2, which was consistent with the reported 3.6 ~ 4.0 GJ·t^{-1} CO_2. When the desorption rate was 90%, L30N50W20 heat duty was 1.335 GJ/t CO_2, with only 33% MEA aqueous. The reasons are summarized as follows. First, the decomposition ΔH_{abs} of [TZ]COO$^-$ was lower than that of -RNHCOO$^-$, CO_2 was primarily present in the form of [TZ]COO$^-$, and NHD could further reduce its decomposition energy barrier, resulting in a significant 69% reduction of Q_{des}. Thus, using short-chain alkyl diamines to synthesize IL with [TZ]H increased the proportion of [TZ]COO$^-$ in the CO_2 absorption products and effectively reduced the energy consumption of CO_2 regeneration. Although long-chain alkyl polyamines (such as tetraethylenepentamines) had a high molar absorption capacity, most CO_2 absorption products were in the form of NCOO$^-$ or –NHCOO$^-$, which could have increased the amount of energy needed to regenerate one unit of CO_2. Second, the lower regeneration temperature and the water content of the CO_2-rich phase reduced the solvent loss, resulting in a 56% reduction of Q_{sol}. Finally, the amount of solvent needed to be regenerated was decreased due to the increased CO_2-rich phase loading. Qsen was also reduced by 67% due to the low specific heat capacity of the CO_2-rich phase.

4. Conclusion

This work synthesized a biphasic solvent based on dual-functionalized IL: [DMAPA][TZ], NHD, and water for industrial CO_2 capture. Under optimal conditions, the solvent exhibited a maximum absorption capacity of 1.95 mol·L^{-1} at a CO_2 partial pressure of 15 kPa. Its CO_2-rich phase accounted for 40 vol% of the total volume, enriching 95.2% of the absorption load to 4.65 mol·L^{-1}. Its lower phase viscosity of 70.7 mPa·s was significantly lower than that of most anhydrous solvents. The desorption efficiency could reach 92.3% when heated at 373 K for 10 min without the CO_2-lean phase, but it remained at 83% after ten regeneration cycles. The effective recoverability with low regeneration energy consumption under these circumstances, 1.335 GJ·t^{-1} CO_2, was evidence of its sustainability. This is 67% less than that of MEA/

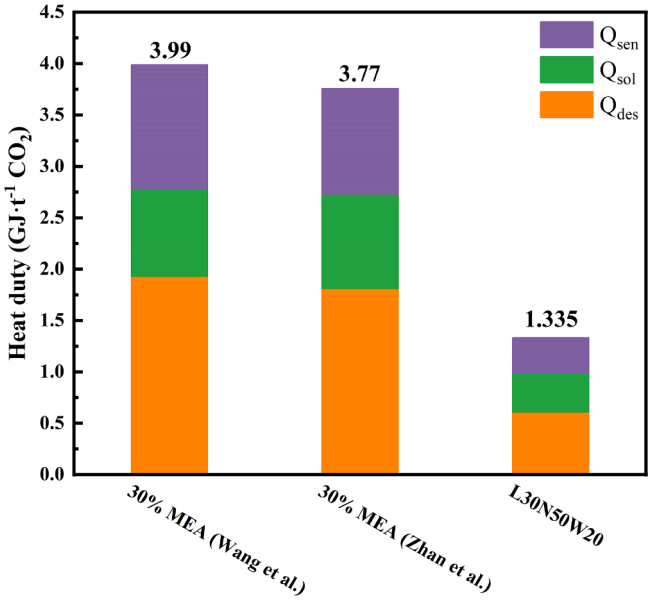

Fig. 12. Thermodynamics of varied solutions. The MEA data were obtained from Wang et al. [14]. and Zhan et al. [8].

water. According to the results of ^{13}C NMR, both anions and cations of [DMAPA][TZ] can react with CO_2 to form carbamate, which further hydrolyzes with H_2O to form HCO_3^- and CO_3^{2-}. NHD accelerates the absorption and desorption reaction rate, increases the absorption load, and acts as a phase-splitting agent to promote phase transition. In addition, its co-solvent was non-volatile, non-flammable, and highly stable. Our research is still in the lab but offers a new method for creating CO_2 absorption solvents. We will conduct a pilot study of the CO_2 capture process in our future work.

CRediT authorship contribution statement

Jiaming Mao: Data curation, Formal analysis, Investigation, Methodology, Visualization, Software, Validation, Writing – original draft. **Yanbin Yun:** Writing – review & editing. **Meng Li:** Data curation, Formal analysis, Investigation. **Wenli Liu:** Methodology, Visualization. **Chang Li:** Data curation, Formal analysis. **Liming Hu:** Software, Validation. **Jia Liu:** Investigation. **Lihua Wang:** Writing – review & editing. **Chunli Li:** Writing – review & editing.

Declaration of Competing Interest

The authors declare that they have no known competing financial interests or personal relationships that could have appeared to influence the work reported in this paper.

Data availability

Data will be made available on request.

Acknowledgments

This work was supported by the National Key Research and Development Program of China (No.2018YFB0604302-03) and Beijing Synling Technology Co. Ltd (2019-HXFW-HJ-0008). The authors thank Ruirong Zhang from Shiyanjia Lab (www.shiyanjia.com) for the NMR analysis.

Appendix A. Supplementary material

Supplementary data to this article can be found online at https://doi.org/10.1016/j.seppur.2023.123722.

References

[1] W.F. Jiang, X.S. Li, G. Gao, F. Wu, C. Luo, L.Q. Zhang, Advances in applications of ionic liquids for phase change CO_2 capture, Chem. Eng. J. 445 (2022), 136767.
[2] W.F. Jiang, F. Wu, G. Gao, X.S. Li, L.Q. Zhang, C. Luo, Absorption performance and reaction mechanism study on a novel anhydrous phase change absorbent for CO_2 capture, Chem. Eng. J. 420 (2021) 11.
[3] Y.F. Li, L. Wang, P.R. Jin, X. Song, X.Y. Zhan, Removal of carbon dioxide from pressurized landfill gas by physical absorbents using a hollow fiber membrane contactor, Chem. Eng. Process. 121 (2017) 149–161.
[4] D. Hospital-Benito, J. Lemus, C. Moya, R. Santiago, V.R. Ferro, J. Palomar, Techno-economic feasibility of ionic liquids-based CO_2 chemical capture processes, Chem. Eng. J. 407 (2021) 9.
[5] A.I. Papadopoulos, F.A. Perdomo, F. Tzirakis, G. Shavalieva, I. Tsivintzelis, P. Kazepidis, E. Nessi, S. Papadokonstantakis, P. Seferlis, A. Galindo, G. Jackson, C. S. Adjiman, Molecular engineering of sustainable phase-change solvents: from digital design to scaling-up for CO_2 capture, Chem. Eng. J. 420 (2021) 13.
[6] J.S. Liu, J. Qian, Y. He, Water-lean triethylenetetramine/N, N-diethylethanolamine/n-propanol biphasic solvents: phase-separation performance and mechanism for CO_2 capture, Sep. Purif. Technol. 289 (2022) 13.
[7] M.N. Tao, J.Z. Gao, W. Zhang, Y. Li, Y. He, Y. Shi, A novel phase-changing nonaqueous solution for CO_2 capture with high capacity, thermostability, and regeneration efficiency, Ind. Eng. Chem. Res. 57 (2018) 9305–9312.
[8] X. Zhan, B. Lv, K. Yang, G. Jing, Z. Zhou, Dual-functionalized ionic liquid biphasic solvent for carbon dioxide capture: high-efficiency and energy saving, Environ. Sci. Technol. 54 (2020) 6281–6288.
[9] Z. Chen, B. Yuan, G. Zhan, Y. Li, J. Li, J. Chen, Y. Peng, L. Wang, C. You, J. Li, Energy-efficient biphasic solvents for industrial carbon capture: role of physical solvents on CO_2 absorption and phase splitting, Environ. Sci. Technol. 56 (2022) 13305–13313.
[10] C. Nwaoha, R. Idem, T. Supap, C. Saiwan, P. Tontiwachwuthikul, W. Rongwong, M. J. Al-Marri, A. Benamor, Heat duty, heat of absorption, sensible heat and heat of vaporization of 2-Amino-2-Methyl-1-Propanol (AMP), Piperazine (PZ) and Monoethanolamine (MEA) tri-solvent blend for carbon dioxide (CO_2) capture, Chem. Eng. Sci. 170 (2017) 26–35.
[11] X.F. Wang, N.G. Akhmedov, D. Hopkinson, J. Hoffman, Y.H. Duan, A. Egbebi, K. Resnik, B.Y. Li, Phase change amino acid salt separates into CO_2-rich and CO_2-lean phases upon interacting with CO_2, Appl. Energy 161 (2016) 41–47.
[12] F. Liu, Y. Shen, L. Shen, C. Sun, L. Chen, Q.L. Wang, S.J. Li, W. Li, Novel amino-functionalized ionic liquid/organic solvent with low viscosity for CO_2 capture, Environ. Sci. Technol. 54 (2020) 3520–3529.
[13] M.T. Zaky, M.I. Nessim, M.A. Deyab, Synthesis of new ionic liquids based on dicationic imidazolium and their anti-corrosion performances, J. Mol. Liq. 290 (2019) 7.
[14] L.D. Wang, S.S. Liu, R.J. Wang, Q.W. Li, S.H. Zhang, Regulating phase separation behavior of a DEEA-TETA biphasic solvent using sulfolane for energy-saving CO_2 capture, Environ. Sci. Technol. 53 (2019) 12873–12881.
[15] M.W. Arshad, H.F. Svendsen, P.L. Fosbol, N. von Solms, K. Thomsen, Equilibrium total pressure and CO_2 solubility in binary and ternary aqueous solutions of 2-(diethylamino)ethanol (DEEA) and 3-(methylamino)propylamine (MAPA), J. Chem. Eng. Data 59 (2014) 764–774.
[16] Q.S. Huang, G.H. Jing, X.B. Zhou, B.H. Lv, Z.M. Zhou, A novel biphasic solvent of amino-functionalized ionic liquid for CO_2 capture: High efficiency and regenerability, J. CO_2 Util. 25 (2018) 22–30.
[17] W.X. Kong, B.H. Lv, G.H. Jing, Z.M. Zhou, How to enhance the regenerability of biphasic absorbents for CO_2 capture: an efficient strategy by organic alcohols activator, Chem. Eng. J. 429 (2022) 11.
[18] X.S. Li, J. Liu, W.F. Jiang, G. Gao, F. Wu, C. Luo, L.Q. Zhang, Low energy-consuming CO_2 capture by phase change absorbents of amine/alcohol/H_2O, Sep. Purif. Technol. 275 (2021) 7.
[19] S.J. Zeng, X. Zhang, L.P. Bai, X.C. Zhang, H. Wang, J.J. Wang, D. Bao, M.D. Li, X. Y. Liu, S.J. Zhang, Ionic-liquid-based CO_2 capture systems: structure, interaction and process, Chem. Rev. 117 (2017) 9625–9673.
[20] C.M. Wang, H.M. Luo, D.E. Jiang, H.R. Li, S. Dai, Carbon dioxide capture by superbase-derived protic ionic liquids, Angew. Chem.-Int. Edit. 49 (2010) 5978–5981.
[21] F. Zhang, K.X. Gao, Y.N. Meng, M. Qi, J. Geng, Y.T. Wu, Z.B. Zhang, Intensification of dimethyaminoethoxyethanol on CO_2 absorption in ionic liquid of amino acid, Int. J. Greenh. Gas Control 51 (2016) 415–422.
[22] D. Camper, J.E. Bara, D.L. Gin, R.D. Noble, Room-temperature ionic liquid-amine solutions: tunable solvents for efficient and reversible capture Of CO_2, Ind. Eng. Chem. Res. 47 (2008) 8496–8498.
[23] M. Hasib-ur-Rahman, M. Siaj, F. Larachi, CO_2 capture in alkanolamine/room-temperature ionic liquid emulsions: a viable approach with carbamate crystallization and curbed corrosion behavior, Int. J. Greenh. Gas Control 6 (2012) 246–252.
[24] J.X. Ye, C.K. Jiang, H. Chen, Y. Shen, S.H. Zhang, L.D. Wang, J.M. Chen, Novel biphasic solvent with tunable phase separation for CO_2 capture: role of water content in mechanism, kinetics, and energy penalty, Environ. Sci. Technol. 53 (2019) 4470–4479.
[25] F. Liu, Y. Shen, L. Shen, Y.C. Zhang, W.Q. Chen, Q.L. Wang, S.J. Li, S.A. Zhang, W. Li, Sustainable ionic liquid organic solution with efficient recyclability and low regeneration energy consumption for CO2 capture, Sep. Purif. Technol. 275 (2021) 8.
[26] N. Aziz, R. Yusoff, M.K. Aroua, Absorption of CO_2 in aqueous mixtures of N-methyldiethanolamine and guanidinium tris(pentafluoroethyl)trifluorophosphate ionic liquid at high-pressure, Fluid Phase Equilib. 322 (2012) 120–125.
[27] H.C. Zhou, X. Xu, X.C. Chen, G.R. Yu, Novel ionic liquids phase change solvents for CO_2 capture, Int. J. Greenh. Gas Control 98 (2020) 8.
[28] S. Seo, M. Quiroz-Guzman, M.A. DeSilva, T.B. Lee, Y. Huang, B.F. Goodrich, W. F. Schneider, J.F. Brennecke, Chemically tunable ionic liquids with aprotic heterocyclic anion (AHA) for CO_2 capture, J. Phys. Chem. B 118 (2014) 5740–5751.
[29] X.T. Hu, X.M. Yang, L.F. Chen, M.C. Mei, Z. Song, Z.F. Fei, P.J. Dyson, Z.W. Qi, Elucidating the transition between CO_2 physisorption and chemisorption in 1,2,4-triazolate ionic liquids at a molecular level, Chem. Eng. J. 435 (2022) 10.
[30] A.L. Revelli, F. Mutelet, J.N. Jaubert, High carbon dioxide solubilities in lmidazolium-based ionic liquids and in poly(ethylene glycol) dimethyl ether, J. Phys. Chem. B 114 (2010) 12908–12913.
[31] M. Ramdin, Q. Chen, S.P. Balaji, J.M. Vicent-Luna, A. Torres-Knoop, D. Dubbeldam, S. Calero, T.W. de Loos, T.J.H. Vlugt, Solubilities of CO_2, CH_4, C_2H_6, and SO_2 in ionic liquids and Selexol from Monte Carlo simulations, J. Comput. Sci. 15 (2016) 74–80.
[32] Z. Kapetaki, P. Brandani, S. Brandani, H. Ahn, Process simulation of a dual-stage Selexol process for 95% carbon capture efficiency at an integrated gasification combined cycle power plant, Int. J. Greenh. Gas Control 39 (2015) 17–26.
[33] T.J. Simons, T. Verheyen, E.I. Izgorodina, R. Vijayaraghavan, S. Young, A. K. Pearson, S.J. Pas, D.R. MacFarlane, Mechanisms of low temperature capture and regeneration of CO_2 using diamino protic ionic liquids, Phys. Chem. Chem. Phys. 18 (2016) 1140–1149.
[34] Z.H. Tu, P.P. Liu, X.M. Zhang, M.Z. Shi, Z. Zhang, S.L. Luo, L.P. Zhang, Y.T. Wu, X. B. Hu, Highly-selective separation of CO_2 from N_2 or CH_4 in task-specific ionic liquid membranes: facilitated transport and salting-out effect, Sep. Purif. Technol. 254 (2021) 9.

[35] T. Oncsik, R. Vijayaraghavan, D.R. MacFarlane, High CO_2 absorption by diamino protic ionic liquids using azolide anions, Chem. Commun. 54 (2018) 2106–2109.
[36] Y.S. Sistla, A. Khanna, CO_2 absorption studies in amino acid-anion based ionic liquids, Chem. Eng. J. 273 (2015) 268–276.
[37] Y.T. Varma, D.S. Agarwal, A. Sarmah, L. Joshi, R. Sakhuja, D.D. Pant, Solvent effects on the absorption and emission spectra of novel (E)-4-((4-(heptyloxy) phenyl)diazenyl)benzyl (((9H-fluoren-9-yl) methoxy)carbonyl)-D-alaninate (Fmoc-al-az): Determination of dipole moment by experimental and theoretical study, J. Mol. Struct. 1129 (2017) 248–255.
[38] Z.H. Tu, M.Z. Shi, X.M. Zhang, P.P. Liu, Y.T. Wu, X.B. Hu, Selective membrane separation of CO_2 using novel epichlorohydrin-amine-based crosslinked protic ionic liquids: Crosslinking mechanism and enhanced salting-out effect, J. CO_2 Util. 46 (2021), 101473.
[39] S.Y. Zheng, J.H. Zhou, S.B. Wang, Y.J. Wang, S.Q. Liu, G.Y. Du, D. Zhang, J.M. Fu, J. Lin, Z.L. Wu, Q. Zheng, J.T. Yang, Water-triggered spontaneously solidified adhesive: from instant and strong underwater adhesion to in situ signal transmission, Adv. Funct. Mater. 32 (2022) 10.
[40] Y. Tian, J.N. Hong, D.Y. Cao, S.F. You, Y.Z. Song, B.W. Cheng, Z.C. Wang, D. Guan, X.M. Liu, Z.P. Zhao, X.Z. Li, L.M. Xu, J. Guo, J. Chen, E.G. Wang, Y. Jiang, Visualizing Eigen/Zundel cations and their interconversion in monolayer water on metal surfaces, Science 377 (2022) 315–319.
[41] J.T. Wang, S.F. Wang, Q.P. Xin, Y.F. Li, Perspectives on water-facilitated CO_2 capture materials, J. Mater. Chem. A 5 (2017) 6794–6816.
[42] K.X. Wei, L. Xing, Y.C. Li, T. Xu, Q.W. Li, L.D. Wang, Heteropolyacid modified Cerium-based MOFs catalyst for amine solution regeneration in CO_2 capture, Sep. Purif. Technol. 293 (2022) 8.
[43] L. Xing, K.X. Wei, Q.W. Li, R.J. Wang, S.H. Zhang, L.D. Wang, One-step synthesized SO_4^{2-}/ZrO_2-HZSM-5 solid acid catalyst for carbamate decomposition in CO_2 capture, Environ. Sci. Technol. 54 (2020) 13944–13952.